Hamburger Beiträge
zur Angewandten Mathematik

Optimal control of the temperature in a catalytic converter

Ingenuin Gasser, Martin Rybicki, Winnifried Wollner

Nr. 2013-07
July 2013

OPTIMAL CONTROL OF THE TEMPERATURE IN A CATALYTIC CONVERTER

INGENIUN GASSER, MARTIN RYBICKI, WINNIFRIED WOLLNER*

Abstract. This paper is concerned with the optimization of the dynamics of the gas flow in an exhaust pipe. As prototypical question the start up heating of the catalytic converter is considered. Here reaching the optimal temperature in the converter rapidly competes against the costs, i.e., releasing too much unburnt fuel in the exhaust gases. The underlying model is a one dimensional small Mach number asymptotic gas dynamic model for a mixture of burnt and unburnt gas, formulated on a network consisting of the various pieces of the exhaust tube. For the optimization, adjoint calculus is applied on the continuous level. The resulting system is then discretized. Finally, numerical examples show the validity of this approach.

Key words. Catalytic converter, Combustion, Exhaust pipe, Gas dynamics, Gas dynamics network, Optimization, Small Mach number

AMS subject classifications. 35Q35, 35Q93, 80A25

1. Introduction. The control and the reduction of the emission caused by vehicles is an import issue over the last 5 decades. The first restrictions were introduced by the government of California (USA) in the early 1960s. In 1970 the European Community passed first laws regarding exhaust gas pollution. Today, there is the *Euro 5* standard and the next *Euro 6* standard will be compulsory in 2014 in Europe. Similar severe restrictions hold in North America. Many other countries nowadays use or introduce similar restrictions.

For the reduction of the concentration of CO, NO_x and C_xH_y in the exhaust gas, there is a classical technical solution, namely (mostly) two catalytic converters installed in the exhaust pipe system. The function of the catalytic converters depends strongly on the temperature in the converters. There is a lower limit (about 600 degrees Celsius) for a good function and an upper limit to avoid damages. In particular, right after engine start there is a critical time interval where the temperature in the converters is not high enough. A method of heating after the engine start is the combustion of unburnt gas in the catalytic converters. Modern exhaust systems can control the ratio of oxygen and fuel in the combustion chamber of the engine. By choosing a ratio with more fuel and less oxygen some unburnt fuel flows to the catalytic converters where it can be used for an exothermic reaction. Clearly, there is a competition between reaching the optimal converter temperature fast and using very little unburnt fuel in the exhaust gas. This choice is the main issue in this paper. We show, how to compute an optimal inflow distribution of unburnt gas (into the exhaust tube), with respect to the cost function, that will be presented later.

To face this problem, one has to model, appropriately, the gas dynamics in the exhaust pipe and the heat dynamics in the converters. In addition, we not only need an appropriate model but also a model which allows fast direct simulations in order to be able to apply optimization tools; that typically need several simulations during the optimization.

There is not much mathematical literature on the modelling of gas dynamic issues in an exhaust pipe in the literature. We mention [20, 14, 4] on studies regarding the temperature in the converter based on more complex chemical models, with assumed

*Universität Hamburg, Hamburg, Germany.

homogeneous gas dynamics. Furthermore, we mention fully compressible fluid dynamic models for the exhaust tube, where the aim is not primarily the determination of the converter temperature but the computation of sound waves (see e.g. [11, 15]) or mechanical properties of the exhaust tube (see e.g. [12, 16]).

A model which promises to be appropriate was developed recently in [6, 7]. We shortly summarize the main features of this model:

- The model is one dimensional in space. The spacial extension is along the exhaust tube and all the values are mean values over the (non constant) cross section.
- The basis is a fully compressible multi component gas dynamic model including surface friction and heat transfer through the surface, i.e. the exhaust tube walls.
- Since in this application the flow velocities are small (compared to the speed of sound), i.e., the Mach number is small; a small Mach number asymptotic model is used in order to rule out sound waves. This reduces the simulation times significantly.
- We use two gas components to model the underlying complex chemistry, namely burnt and unburnt gas. However, the crucial quantity for the heating in the catalytic converters is the total heat release of the chemical reaction which can be easily included in such a simple two component reaction model.
- The exhaust tube is modeled as a network of tubes with constant cross section.

Neither in the pre-asymptotic hyperbolic model, nor in the asymptotic (hyperbolic-elliptic-like) model we have a well-posedness theory. However, assuming existence of a unique solution and differentiability with respect to the inflow of unburnt gas, we will derive a system of differential equations yielding the continuous adjoint to the calculated flow. These will be used to find an optimal inflow profile using a projected gradient method.

We remark that even in the pre-asymptotic regime, i.e., for hyperbolic systems, questions of uniqueness, differentiability, and optimality conditions are a field of active research. To give an impression of the different questions under consideration see, e.g., [9] for well-posedness of hyperbolic problems on networks, [22] for sensitivity analysis of hyperbolic conservation laws, [8, 13] for optimization problems with hyperbolic equations on networks, [1] for control of Burgers equation with vanishing viscosity, or [2] for the control of unsteady compressible fluids.

However, the asymptotic model, with the above mentioned properties, allows direct simulations almost in real time on a standard laptop computer. The model derived in [6] was built on the basis of models proposed in [19, 18]. In order to validate the models accuracy, we compared its numerical solutions to the ones of the fully hyperbolic problem and found a good agreement (see [6]).

Although it seems that we have drastically reduced the complexity of the model from a mathematical point of view, we still have a multi component nonlinear system of PDE's on a network. To do optimization on such a model is still a highly challenging topic. We mention only a few papers where similarly complex issues where studies. In [10] optimization of the gas flow in a pipeline is considered, whereas the optimal control for traffic flow is discussed in [8]. In [5] the optimal control of glass cooling is studied.

The paper is organized as follows. In section 2, we introduce the model, which was derived in its main parts in [6]. In section 3, we define the optimization problem. In section 4, we derive the optimality system. Section 5 is devoted to the discretization.

Finally, in section 6, we present numerical examples.

2. Model. The following dimensionless model describes the gas dynamics in an exhaust pipe.

$$
\begin{aligned}
(A\rho)_t + (A\rho u)_x &= 0,\\
(A\rho u)_t + (A\rho u^2)_x + \frac{1}{\varepsilon}Ap_x &= -C_f\rho\frac{u|u|}{2} - C_cA\chi\rho u,\\
(A\rho T + \varepsilon\frac{R}{c_v}A\rho\frac{u^2}{2})_t + (A\rho uT + \varepsilon\frac{R}{c_v}Aup)_x &= -h(T - T_{\text{Wall}}) + q_0A\chi\rho zK(T),\\
(A\rho z)_t + (A\rho uz)_x &= -A\chi\rho zK(T),\\
p &= \rho T,
\end{aligned}
\tag{2.1}
$$

with the unknows ρ, u, p, T, z as the density, velocity, pressure, temperature, and the ratio of unburnt gas, respectively. The terms on the left hand side originate from the one-dimensional Euler equations of gas dynamic in a pipe with variable cross section $A = A(x)$. By the terms on the right hand side, we describe the main physical effects which influence the dynamics of the gas. The first equation is the conservation of mass. On the right hand side of the second equation (momentum balance) we first have a wall friction (wall friction coefficient C_f) and secondly a local friction (honeycomb structure friction coefficient C_c) due to the honeycomb structure of the catalyst (locality is denoted by the indicator function χ). In the third equation (energy balance) we have, on one hand, energy loss due to heat transfer with the wall (heat transfer coefficient h, wall temperature T_{Wall}), and, on the other hand, an energy gain due to the local exothermic reaction in the catalytic converter (heat release coefficient q_0). The parameters c_v and R denote the specific heat at constant volume and the ideal gas constant, respectively. The fourth equation (reaction balance) describes the dynamics of the the ratio of unburnt gas z in the pipe. The temperature dependent reaction rate $K(T)$ is modeled by *Arrhenius' law*. Lastly, we have the ideal gas law as a closing relation.

The parameter $\varepsilon := \gamma M^2$ equals the product of the adiabatic exponent and the square of the Mach number, and is known to be small (see [6]).

The numerical simulation of the fully compressible model (2.1) is (although it is "only" 1D) costly. In [6] it is shown that for many purposes there is a simplified model to simulate gas dynamics more efficiently on the basis of (2.1). There are two major steps in the derivation of this simplified model:

1. Rather than introducing artificial intervals for a smooth change of the cross section A, one divides the exhaust pipe into pipes with constant cross sections and treat the whole system as a network. This has two major advantages:
   (a) Avoiding strong changes of A on small x-intervals, we can use larger step sizes in space (and therefore, also in time).
   (b) The coupling conditions at the junctions, allow to include models for pressure losses caused by the pipe's geometry.
2. The flow in the exhaust pipe is of low Mach number (M), and (in this application) one is not interested in the propagation of sound waves, but mainly in the temperature in the catalyst. Thus, one is able to simplify the model by a small Mach number asymptotics ($\varepsilon \to 0$). This will lead to the simplified model (2.2), which is computationally much cheaper than the fully hyperbolic model (2.1), due to much larger step sizes in time given by the CFL condition.

See [6] for the detailed derivation and comparison with the original model (2.1). The final version of our asymptotic model is the following:

$$
\begin{aligned}
\rho^i_t + (v^i + Q^i)\rho^i_x &= -q^i\rho^i,\\
z^i_t + (v^i + Q^i)z^i_x &= -\chi^i z^i K(T^i),\\
v^i_t &= \Phi^i/R^i(0),\\
p_0 &= \rho^i T^i,
\end{aligned}
\tag{2.2}
$$

with unknowns $\rho^i = \rho^i(x,t), v^i = v^i(t), z^i = z^i(x,t), T^i = T^i(x,t)$ as the density, time dependent velocity component, the ratio of unbrunt gas and the temperature for the i-th pipe, respectively. Before we give definition for the other variables, let us first discuss the structure of the model. We see that instead of four coupled PDEs in (2.1) we have now only a system of two PDEs and one Integro-ODE. The super-index $i \in \{1, \dots, n_P\}$ denotes the pipe number, where n_P is the amount of pipes in total. Since we have to differentiate between pipes that do and do not have a catalytic converter, we denote multiply terms, that only occur in pipes that have a catalyst, with the indicator function χ^i.

$$
\chi^i = \begin{cases} 1 & \text{pipe } i \text{ has a catalyst} \\ 0 & \text{otherwise} \end{cases}
\tag{2.3}
$$

Furthermore, we have to define some terms in the equations (2.2). All values for the parameters, can be found in the appendix A.

1. The velocity u is now split into the space independent velocity component v and the aggregated energy balance Q.

$$
u^i(x,t) = v^i(t) + Q^i[\rho^i, z^i](x,t) = v^i(t) + \int_0^x q^i[\rho^i, z^i](y,t)dy,
\tag{2.4}
$$

$$
\begin{aligned}
q^i[\rho^i, z^i](x,t) := \frac{1}{\gamma p_0} \big[&-h(T^i(x,t) - T^i_{\text{Wall}}(x,t))\\
&+\chi^i q_0 \rho^i(x,t) z^i(x,t) K(T^i(x,t))\big],
\end{aligned}
\tag{2.5}
$$

   with p_0 zero order pressure in the small Mach number asymptotics and

$$
T^i_{\text{Wall}}(x,t) := \frac{1}{2}\left(T^i(x,t) + T_{out}\right),
\tag{2.6}
$$

   where T_{out} is the scaled outside temperature.
2. The reactions rate K, which depends on the temperature/density of the gas mixture is defined in the following way:

$$
K(T^i) := \frac{\tilde{K}_0 x_r}{u_r} \exp\left(-\frac{\tilde{T}^+}{T_r T^i}\right) = \frac{\tilde{K}_0 x_r}{u_r} \exp\left(-\frac{\tilde{T}^+}{T_r p_0}\rho^i\right) =: K_\rho(\rho^i)
\tag{2.7}
$$

   with $\tilde{E}^+ = R\tilde{T}^+$ as the activation energy.
3. The right hand side of the third equation is defined (with $q^i(x,t) = q^i[\rho^i, z^i](x,t)$

and $Q^i(x,t) = Q^i[\rho^i, z^i](x,t))$ as follows:

$$(R^i(x))(t) := \int_x^{L^i} \rho^i(y,t)dy \tag{2.8}$$

$$\begin{aligned}\Phi^i[\rho^i, z^i, v^i](t) := {} & p^i_{1l}(t) - p^i_{1r}(t) - \int_0^{L^i} \rho^i(x,t)Q^i_t(x,t)dx \\ & - \int_0^{L^i} \rho^i(x,t)(v^i(t) + Q^i(x,t))q^i(x,t)dx \\ & - C_f \int_0^{L^i} \rho^i(x,t)\frac{(v(t)^i + Q^i(x,t))|v(t)^i + Q^i(x,t)|}{2}dx \\ & - \chi^i C_c \int_0^{L^i} \rho^i(x,t)(v^i(t) + Q^i(x,t))\ dx.\end{aligned} \tag{2.9}$$

The index set $I_{cc} \subset 1, \ldots, n_P$ contains all pipes the contain a catalytic converter. In order to describe the heating of the catalytic converter, we need to introduce an equation which models the evolution of the temperature of the catalyst. We model the temperature of the catalytic converter T^i_c as a result of the heat exchange among catalyst temperature T^i_c and the average gas temperature T^i_{Gas} in the i-th pipe.

$$T^i_{\text{Gas}}(t) := \frac{1}{L^i} \int_0^{L^i} T^i(x,t)dx. \tag{2.10}$$

We choose the following ODE, for all pipes $i \in I_{cc}$, to model this relation.

$$(T^i_c(t))_t = -h_c(T^i_c(t) - T^i_{\text{Gas}}(t)), \tag{2.11}$$

and we substitute q^i from (2.5) by

$$\begin{aligned}q^i[\rho^i, z^i, T^i_c] := \frac{1}{\gamma p_0} \big[& -h(T^i - T^i_{\text{Wall}}) \\ & + \chi^i \left(-h_c(T^i(t) - T^i_c(t)) + q_0 \rho^i z^i K(T^i) \right) \big],\end{aligned} \tag{2.12}$$

including the heat exchange with the catalytic converter in the energy balance q^i.

2.1. The summarized model. To summarize, we consider for our optimization task the following model to describe the physics in an exhaust pipe:

$$\begin{aligned}\rho^i_t + (v^i + Q^i)\rho^i_x &= -q^i\rho^i, \\ z^i_t + (v^i + Q^i)z^i_x &= -\chi^i z^i K(T^i), \\ v^i_t &= \Phi^i / R^i(0), \\ (T^j_c)_t &= -h_c(T^j_c - T^j_{\text{Gas}}),\end{aligned} \tag{2.13}$$

for all pipes $i = 1, \dots, n_P$, $j \in I_{cc}$ and $(x,t) \in (0, L^i) \times (0, t_{end})$, with closing relation

$$\rho^i(x,t)T^i(x,t) = p_0, \tag{2.14}$$

for all pipes $i = 1, \dots, n_P$ and $(x,t) \in [0, L^i] \times [0, t_{end}]$, initial conditions

$$\rho^i(x,0) = \rho^i_{ic}(x), \qquad z^i(x,0) = z^i_{ic}(x), \qquad v^i(0) = v^i_{ic}, \qquad T^j_c(0) = T^j_{c\,ic}, \tag{2.15}$$

for all pipes $i = 1, \dots, n_P$, $j \in I_{cc}$ and $x \in [0, L^i]$, boundary conditions for all times $t \in [0, t_{end}]$

$$\rho^1(0,t) = \rho_l(t), \qquad z^1(0,t) = z_l(t), \tag{2.16}$$

and coupling conditions for all pipes $i = 2, \dots, n_P$

$$\rho^{i-1}(L^{i-1}, t) = \rho^i(0,t), \qquad z^{i-1}(L^{i-1}, t) = z^i(0,t). \tag{2.17}$$

REMARK 2.1. *There are additional physical boundary conditions we need to prescribe, i.e., the pressure value at the exhaust pipe's very left end very right end.*

$$p^1(0,t) = p_l(t) = p_0 + \varepsilon p_{1l}(t), \qquad p^{n_P}(L^{n_P}, t) = p_r(t) = p_0 + \varepsilon p_{1r}(t). \tag{2.18}$$

For the mathematical model (2.13) these are just parameters (which appear in Φ^i, see (2.9)). Therefore it is not mentioned in the model description. Since we also need pressure values at the junctions, we need to prescribe a coupling condition for the pressure value.

$$p^{i-1}(L^{i-1}, t) = p^i(0,t) + f_{ext}. \tag{2.19}$$

See [6] or [3, 17] for the definition of the pressure loss term f_{ext}. The numerical computation of all pressure values at each pipe end for each time step is not trivial and explained in detail in [6].

3. The Optimization Problem.

3.1. What do we want to optimize?. As already mentioned in the introduction, the exothermic reaction of the unburnt gas has a major impact on the gas temperature in the catalyst. The desired reactions in the catalyst take place best if a certain temperature is achieved. More precisely the catalyst is not functioning if the temperature is below a certain threshold, and may be damaged if a certain critical temperature is exceeded.

It is thus natural to consider an optimization problem to reach a desired temperature T_{opt} by controlling the inflow of unburnt gas z_l. We will neglect the natural constraints induced by avoiding damage in this article.

In order to formulate this optimization task, we first need a cost functional. As described above, on the one hand we want to reach the light of temperature in the catalyst, but on the other hand do not want to use too much fuel. We express this by the following cost functional.

$$\mathcal{J}(T^i_c, z_l) := \frac{1}{2} \sum_{i \in I_{cc}} \int_0^{t_{\text{end}}} (T^i_c(t) - T_{opt})^2 dt + \sigma \int_0^{t_{\text{end}}} z_l(t) dt, \tag{3.1}$$

with the additional upper and lower bound for z_l

$$0 \leq z_l(t) \leq z_l^{\max} \quad \forall t \in [0, t_{\text{end}}]. \tag{3.2}$$

We note that the choice of the tracking type term for the temperature is rather arbitrary, but is sufficient for our discussion. However, the choice of an L_1-type term for the unburnt gas is physically well motivated by the linear costs associated with the amount of fuel used.

For the algorithmic realization, we assume that for any nonnegative function $z_l \in L_1(0, t_{\text{end}})$ there is a unique temperature $T_c^i = T(z_l) \in L_2(0, t_{\text{end}})$ given by the model (2.13)-(2.17). This gives rise to the reduced problem to find z_l solving

$$\begin{aligned} \min j(z_l) &= \mathcal{J}(T(z_l), z_l) \\ \text{s.t. } 0 &\leq z_l \leq z_l^{\max}. \end{aligned} \tag{3.3}$$

To solve this numerically, we will apply a projected gradient method in this reduced setting, see Section 5. Before we can do so, we need to calculate the derivatives of the reduced cost functional which we will do in the following section.

In the calculations, we follow the optimize-then-discretize approach, meaning that we will derive the necessary optimality conditions for the continuous problem and then discretize the optimality conditions to obtain a discrete problem, see our discussion in Section 5.

4. The optimality system and its derivation. For the following computation, we need to assume that the velocity $u^i = v^i + Q^i$ is non-negative for all $(x, t) \in [0, L^i] \times [0, t_{\text{end}}]$ in all pipes $i = 1, \ldots, n_P$. Then $|v^i + Q^i| = v^i + Q^i$ in the term Φ. This assumption is fully in correspondence with the application.
Since we want to determine the gradient of our cost functional $\mathcal{J}$ by an adjoint-based method, we need to calculate the adjoint. To do so, we formulate a Lagrangian functional. Let $W := (w^1, \ldots, w^{n_P})$ be the vector of all state variables, i.e., $w^i := (\rho^i, z^i, v^i, T_c^i)$ and $\Lambda := (\lambda^1, \ldots, \lambda^{n_P})$ the vector of all adjoint variables, i.e.,

$\lambda^i := (\xi^i_\rho, \xi^i_z, \xi^i_v, \xi^i_{T_c}, \eta_\rho, \eta_z, \nu^i_\rho, \nu^i_z, \nu^i_v, \nu^i_{T_c}, \zeta^i_\rho, \zeta^i_z)$. Then the Lagrangian functional is

$$\mathcal{L}(W, z_l, \Lambda) = \sum_{i\in I_{cc}} \int_0^{t_{\text{end}}} (T^i_c(t) - T_{opt})^2 dt + \sigma \int_0^{t_{\text{end}}} z_l(t) dt \tag{4.1}$$

$$- \sum_{i=1}^{n_P} \int_0^{t_{\text{end}}} \int_0^{L^i} \xi^i_\rho(\rho^i_t + (v^i + Q^i)\rho^i_x + q^i\rho^i) dx dt \tag{4.2}$$

$$- \sum_{i=1}^{n_P} \int_0^{t_{\text{end}}} \int_0^{L^i} \xi^i_z(z^i_t + (v^i + Q^i)z^i_x + \chi^i z^i K(T^i)) dx dt \tag{4.3}$$

$$- \sum_{i=1}^{n_P} \int_0^{t_{\text{end}}} \xi^i_v \left(v^i_t - \frac{\Phi^i}{R^i(0)} \right) dt \tag{4.4}$$

$$- \sum_{i\in I_{cc}} \int_0^{t_{\text{end}}} \xi^i_{T_c}((T^i_c)_t + h_c(T^i_c - T^i_{\text{Gas}})) dt \tag{4.5}$$

$$- \int_0^{t_{\text{end}}} \eta_\rho(\rho^1(0,t) - \rho_l(t)) dt - \int_0^{t_{\text{end}}} \eta_z(z^1(0,t) - z_l(t)) dt \tag{4.6}$$

$$- \sum_{i=1}^{n_P} \int_0^{L^i} \nu^i_\rho(\rho^i(x,0) - \rho^i_{ic}(x)) dx - \sum_{i=1}^{n_P} \int_0^{L^i} \nu^i_z(z^i(x,0) - z^i_{ic}(x)) dx \tag{4.7}$$

$$- \sum_{i=1}^{n_P} \nu^i_v(v^i(0) - v^i_{ic}) - \sum_{i\in I_{cc}} \nu^i_{T_c}(T^i_c(0) - T^i_{c\,ic}) \tag{4.8}$$

$$- \sum_{i=2}^{n_P} \int_0^{t_{\text{end}}} \zeta^i_\rho \left(\rho^{i-1}(L^{i-1}, t) - \rho^i(0,t) \right) dt \tag{4.9}$$

$$- \sum_{i=2}^{n_P} \int_0^{t_{\text{end}}} \zeta^i_z \left(z^{i-1}(L^{i-1}, t) - z^i(0,t) \right) dt. \tag{4.10}$$

Before starting with the computation, let us have a quick look at the lines of this large term. Line (4.1) is representing the cost functional. Lines (4.2 - 4.5) are the four state equations multiplied with *Lagrangian multipliers* ξ^i_*, integrated over space and time and summed up over all pipes of the network. The last four lines are the boundary conditions muliplied with its Lagragian multipliers η^i_* and integrated over time (4.6), the initial conditions multiplied with its Lagragian multipliers ν^i_* integrated over space (4.7 - 4.8) and the coupling conditions multiplied with its Lagrangian multipliers ζ^i_* and integrated over time (4.9 - 4.10).

We derive the optimality system, by computing the first variation, with respect

to Lagrangian multipliers, state variables and the control quantity, i.e.,

$$
\begin{aligned}
\frac{\delta \mathcal{L}}{\partial \lambda_j^i} &= 0 && \Rightarrow \quad \text{constraints or state equations,} \\
\frac{\partial \mathcal{L}}{\partial w_j^i} &= 0 && \Rightarrow \quad \text{adjoint or co-state equations,} \\
\frac{\partial \mathcal{L}}{\partial z_l}(z_l^* - z_l) &\geq 0 \; \forall \, z_l^* \in [0, z_l^{\max}] && \Rightarrow \quad \text{optimality condition.}
\end{aligned} \tag{4.11}
$$

4.1. Derivation of the optimality condition. Let us start with the derivation of the optimality condition, since this computation is the easiest, since z_l only appears in the terms (4.1) and (4.6). Let δz_l be an arbitrarily chosen L^1-function, such that $0 \leq z_l + \epsilon \delta z_l \leq z_l^{\max}$, for sufficient small $\epsilon > 0$. Then the first variation of the Lagrangian $\mathcal{L}$ with respect to the control z_l in direction δz_l is

$$
\frac{\partial \mathcal{L}(W, z_l, \Lambda)}{\partial z_l}(\delta z_l) = \int_0^{t_{\text{end}}} \delta z_l (\sigma + \eta_z) dt.
$$

Given that (4.11) holds for all feasible test-functions we assert that the inequality in the reduced optimality condition holds pointwise almost everywhere in $[0, t_{\text{end}}]$, by fundamental lemma of calculus of variation (see, e.g., [21] Lemma 2.26). This yields to

$$
\boxed{(\sigma + \eta_z)(z_l^* - z_l) \geq 0 \quad \forall \; 0 \leq z_l^* \leq z_l^{\max}}, \tag{4.12}
$$

which in turn is equivalent to

$$
\sigma + \eta_z \begin{cases} \geq 0 & z_l = 0, \\ = 0 & 0 < z_l < z_l^{\max}, \\ \leq 0 & z_l = z_l^{\max}. \end{cases} \tag{4.13}
$$

4.2. Derivation of the constraints or state equations. In order to obtain the state equations formally, we have to compute the first variations of the Lagrangian functional $\mathcal{L}$ with respect to the Lagrangian multipliers. The computation works just like in the above case. We then obtain the state system consisting of our differential equations (2.13) and our boundary (2.16), initial (2.15) and coupling conditions (2.17).

4.3. Derivation of the adjoint or co-state equations. In this subsection, we will refuse to write super-indices, but compute the first variations for a pipe of length $L = 1$ with a catalytic converter. The computation of the adjoint equations for a pipe without a catalyst is just a special case (no equation for T_c and $C_c = K_0 = 0$). Note that in the case of a single pipe, there are no coupling conditions required. We will deal with this problem in subsection 4.4. The following part is most complicated one, when it comes to computation of the first variations. This is the case, because all state variable except v appear in the functional $Q = Q[\rho, z, T_c]$.

We will only compute the variation for the space-independent velocity component v and the density ρ. The latter is the most sophisticated and includes all techniques that are required for the computation of the variation with respect to the other two variables z and T_c. We start with $\partial \mathcal{L}/\partial v$, since this is the easier of the two cases.

4.3.1. First variation of $\mathcal{L}$ with respect to v. The space independent velocity component v appears in the Lagrangian $\mathcal{L}$ in the density PDE (4.2), the ratio of unburnt gas PDE (4.3) and its own ODE (4.4) such as its initial condition (4.8). One has to keep in mind, that the functional Φ (2.9) has also a v-dependence. So before computing the first variation of $\mathcal{L}$ with respect to v, let us have a closer look at the functional Φ.

$$\begin{aligned}\Phi[\rho, z, v+\epsilon\delta v, T_c] - \Phi[\rho, z, v, T_c] &= -\epsilon\delta v \int_0^1 \left(\rho q + C_f\rho\left((v+Q) + \frac{\epsilon\delta v}{2}\right) + C_c\rho\right) dx \\ &= -\epsilon\delta v \int_0^1 \left(\rho q + C_f\rho(v+Q) + C_c\rho\right) dx - \frac{\epsilon^2\delta v^2}{2}\int_0^1 C_f\rho dx.\end{aligned}$$

We already isolated the term of order ϵ^2, since this term is of higher order and will vanish in the limit $\epsilon \to 0$.

$$\begin{aligned}\frac{\partial\mathcal{L}(W, z_l, \Lambda)}{\partial v}(\delta v) = \lim_{\epsilon\to 0}\frac{1}{\epsilon}\Bigg[&-\int_0^{t_{\text{end}}}\int_0^1 \epsilon\delta v(\xi_\rho\rho_x + \xi_z z_x)dxdt - \epsilon\delta v\eta_v|_{t=0} \\ &- \int_0^{t_{\text{end}}} \xi_v\left(\epsilon\delta v_t + \frac{\epsilon\delta v}{R(0)}\left[\int_0^1 \left(\rho q + C_f\rho(v+Q) + C_c\rho\right) dx\right]\right) \\ &- \int_0^{t_{\text{end}}} \xi_v o(\epsilon)\, dx\Bigg].\end{aligned}$$

Using integration by parts, we shift the time derivative of δv to the co-state. This also leads to an evaluation at the boundaries.

$$-\int_0^{t_{\text{end}}} \xi_v\delta v_t dt = \int_0^{t_{\text{end}}} (\xi_v)_t\delta v dt - \Big[\xi_v\delta v\Big]_{t=0}^{t=t_{\text{end}}}.$$

The limit $\epsilon \to 0$ gives

$$\begin{aligned}\frac{\partial\mathcal{L}(W, z_l, \Lambda)}{\partial v}(\delta v) = \int_0^{t_{\text{end}}} \delta v\Bigg[&(\xi_v)_t - \int_0^1 \xi_\rho\rho_x + \xi_z z_x dx \\ &-\xi_v\frac{1}{R(0)}\left(\int_0^1 \rho q + C_f\rho(v+Q) + C_c\rho dx\right)\Bigg] dt \\ &- \Big[\xi_v\delta v\Big]_{t=0}^{t=t_{\text{end}}} - \eta_v\delta v(0).\end{aligned}$$

Now, we assume the derivative of the Lagragian with respect to v, in the direction δv, to vanish. Since the variation δv is arbitrary, we choose a variation that vanishes at the boundaries, i.e., at $t = 0$ and $t = t_{\text{end}}$. Then we deduce, by the fundamental

theorem of variational calculus, that

$$\boxed{-(\xi_v)_t = -\xi_v S(0) - \int_0^1 \xi_\rho \rho_x + \xi_z z_x dx}, \tag{4.14}$$

with

$$S(x) := \frac{1}{R(0)} \int_x^1 (\rho q + C_f \rho(v+Q) + C_c \rho)\, dy. \tag{4.15}$$

By choosing a variation that vanishes only at one of the end points $t = 0, t = t_{\text{end}}$ we obtain, with the knowledge that (4.14) holds

$$\boxed{\xi_v = 0 \quad \text{for } t = t_{\text{end}}.} \tag{4.16}$$

4.3.2. First variation of $\mathcal{L}$ with respect to ρ. Before the computation of the derivative, let us focus on the dependence of q and Q upon the density ρ. We assume $\rho \geq c > 0$, which is in correspondence with the physics.

$$q[\rho + \epsilon\delta\rho, z, T_c] = \frac{1}{\gamma p_0}\Bigg[- h\left(\frac{p_0}{\rho+\epsilon\delta\rho} - T_{Wall}\right) - h_c\left(\frac{p_0}{\rho+\epsilon\delta\rho} - T_c\right) + q_0(\rho+\epsilon\delta\rho) z K_\rho(\rho+\epsilon\delta\rho)\Bigg]$$

Note that, we will use the notation, given in (2.7), for the reaction rate function. We observe that the density variable and its variation do not appear in a linear way, but as the denominator of a friction and the argument of the reaction rate. In order to subtract the evaluation of q at $\rho + \epsilon\delta\rho$, we have to get rid of these terms. We do this by Taylor expansion:

$$\frac{1}{\rho+\epsilon\delta\rho} = \frac{1}{\rho} - \epsilon\delta\rho\frac{1}{\rho^2} + o(\epsilon),$$
$$K_\rho(\rho+\epsilon\delta\rho) = K_\rho(\rho) + \epsilon\delta\rho K'_\rho(\rho) + o(\epsilon).$$

By replacing these terms with the Taylor expansions, we obtain

$$q[\rho+\epsilon\delta\rho, z, T_c] = q[\rho, z, T_c] + \epsilon\delta\rho\frac{1}{\gamma p_0}\left[\frac{p_0(h+h_c)}{\rho^2} + q_0 z(\rho K'_\rho(\rho) + K_\rho(\rho))\right] + o(\epsilon).$$

By definition of Q, this yields

$$Q[\rho+\epsilon\delta\rho, z, T_c] - Q[\rho, z, T_c] = \int_0^x \epsilon\delta\rho q_\rho dy + o(\epsilon), \tag{4.17}$$

$$Q_t[\rho+\epsilon\delta\rho, z, T_c] - Q_t[\rho, z, T_c] = \int_0^x (\epsilon\delta\rho q_\rho)_t\, dy + o(\epsilon) \tag{4.18}$$

where

$$q_\rho := \frac{1}{\gamma p_0}\left(\frac{p_0(h+h_c)}{\rho^2} + q_0 z(\rho K'_\rho(\rho) + K_\rho(\rho))\right). \tag{4.19}$$

Since the density appears in many terms in the Lagrangian, we will compute the first variation of it step by step. The density does not appear in the cost functional (4.1), hence we start with the ξ_ρ-integral (4.2).

The ξ_ρ-integral (4.2)**.**

$$
\begin{aligned}
&-\int_0^{t_{\text{end}}}\int_0^1 \xi_\rho\big((\rho+\epsilon\delta\rho)_t + (v+Q[\rho+\epsilon\delta\rho,\ldots])(\rho+\epsilon\delta\rho)_x \\
&\qquad + q[\rho+\epsilon\delta\rho,\ldots](\rho+\epsilon\delta\rho)\big)dxdt \\
&\qquad + \int_0^{t_{\text{end}}}\int_0^1 \xi_\rho\big(\rho_t + (v+Q)\rho_x + q\rho\big)dxdt \\
&\qquad = -\int_0^{t_{\text{end}}}\int_0^1 \xi_\rho\Bigg(\epsilon\delta\rho_t + (v+Q)\epsilon\delta\rho_x + q\epsilon\delta\rho + \rho q_\rho\epsilon\delta\rho \\
&\qquad\qquad + \rho_x\int_0^x \epsilon\delta\rho q_\rho dy\Bigg)dxdt + o(\epsilon) \\
&\qquad =: \mathcal{I}_{\xi_\rho}.
\end{aligned}
\tag{4.20}
$$

Our aim is to isolate the variation $\delta\rho$, such that we can apply the fundamental lemma of variational calculus again. Therefore we need to integrate by parts two times (one with respect to the spatial and once with respect to the time component). Furthermore, we need to use the following identity

$$
\int_0^1 f(x)\left(\int_0^x g(y)dy\right)dx = \int_0^1 g(x)\left(\int_x^1 f(y)dy\right)dx
$$

which is a consequence of Fubini's theorem. With this we manipulate (4.20) and obtain

$$
\begin{aligned}
\mathcal{I}_{\xi_\rho} = &\int_0^{t_{\text{end}}}\int_0^1 \epsilon\delta\rho\left((\xi_\rho)_t + (v+Q)(\xi_\rho)_x - q_\rho\left[\rho\xi_\rho + \int_x^1 \xi_\rho\rho_x dy\right]\right)dxdt \\
&- \Big[\int_0^{t_{\text{end}}} \epsilon\delta\rho(v+Q)\xi_\rho dt\Big]_{x=0}^{x=1} - \Big[\int_0^1 \epsilon\delta\rho\xi_\rho dx\Big]_{t=0}^{t=t_{\text{end}}} + o(\epsilon).
\end{aligned}
\tag{4.21}
$$

The ξ_z-integral (4.3)**.** Analog computations as above give

$$
\begin{aligned}
&-\int_0^{t_{\text{end}}}\int_0^1 \xi_z\big(z_t + (v+Q[\rho+\epsilon\delta\rho,\ldots])z_x + zK_\rho(\rho+\epsilon\delta\rho)\big)dxdt \\
&+\int_0^{t_{\text{end}}}\int_0^1 \xi_z\big(z_t + (v+Q)z_x + zK_\rho(\rho)\big)dxdt \\
&= -\int_0^{t_{\text{end}}}\int_0^1 \xi_z\left(z_x\int_0^x \epsilon\delta\rho q_\rho dy + \epsilon\delta\rho z K'_\rho(\rho)\right)dxdt + o(\epsilon) \\
&= -\int_0^{t_{\text{end}}}\int_0^1 \epsilon\delta\rho\left(q_\rho\int_x^1 \xi_z z_x dy + \xi_z z K'_\rho(\rho)\right)dxdt + o(\epsilon).
\end{aligned}
\tag{4.22}
$$

The ξ_v-integral (4.4)**.** This is the most technical part, since ρ appears in this term so often. Let us develop this step by step. First, let us have a look on the density integral in the denominator. By Taylor expansion we obtain:

$$\begin{aligned}\frac{1}{\int_0^1 \rho+\epsilon\delta\rho dx} &= \frac{1}{\int_0^1 \rho dx} - \int_0^1 \epsilon\delta\rho dx \frac{1}{\left(\int_0^1 \rho dx\right)^2} + o(\epsilon)\\ &= \frac{1}{R(0)} - \frac{1}{R(0)^2}\int_0^1 \epsilon\delta\rho dx + o(\epsilon).\end{aligned}$$

The term Φ evaluated at $\rho+\epsilon\delta\rho$, will have the following form:

$$\Phi[\rho+\epsilon\delta\rho,\ldots] = \Phi[\rho,\ldots] + \epsilon\Phi_\rho[\delta\rho;\rho,\ldots] + o(\epsilon).$$

We will compute Φ_ρ in detail later. Let us first have a look on the whole integral containing ξ_v.

$$\begin{aligned}&-\int_0^{t_{\text{end}}} \xi_v\left(v_t - \frac{1}{\int_0^1 \rho+\epsilon\delta\rho dx}\Phi[\rho+\epsilon\delta\rho,\ldots]\right)dt + \int_0^{t_{\text{end}}} \xi_v\left(v_t - \frac{1}{\int_0^1 \rho dx}\Phi[\rho,\ldots]\right)dt\\ &= \int_0^{t_{\text{end}}} \xi_v\left(\frac{1}{R(0)}\epsilon\Phi_\rho - \frac{1}{R(0)^2}\int_0^1 \epsilon\delta\rho dx\ \Phi\right)dt + o(\epsilon) =: I \qquad (4.23)\end{aligned}$$

The term $\epsilon\Phi_\rho$ consists of all the terms in which ϵ appears linearly, when evaluating Φ at $\rho+\epsilon\delta\rho$. We will now compute those terms. We therefore split Φ in several parts.

$$\Phi[\rho,z,v,T_c] = p_{1l} - p_{1r} - \overbrace{\int_0^1 \rho Q_t dx}^{=:\Phi_1[\rho,z,T_c]} - \overbrace{\int_0^1 \rho(v+Q)q dx}^{=:\Phi_2[\rho,z,v,T_c]} \qquad (4.24)$$

$$\underbrace{-C_f\int_0^1 \rho\frac{(v+Q)^2}{2}dx}_{=:\Phi_3[\rho,z,v,T_c]} \underbrace{-C_c\int_0^1 \rho(v+Q)dx}_{=:\Phi_4[\rho,z,v,T_c]} \qquad (4.25)$$

We start now with the computation of $-\Phi_i[\rho+\epsilon\delta\rho,z,v,T_c]+\Phi_i[\rho,z,v,T_c]$.

$$\begin{aligned}&-\Phi_1[\rho+\epsilon\delta\rho,z,T_c]+\Phi_1[\rho,z,T_c]\\ &\qquad = -\int_0^1 (\rho+\epsilon\delta\rho)Q_t[\rho+\epsilon\delta\rho,\ldots]dx + \int_0^1 \rho Q_t dx\\ &\qquad = -\int_0^1 \epsilon\delta\rho Q_t + [\epsilon\delta\rho q_\rho]_t R(x)dx + o(\epsilon),\end{aligned} \qquad (4.26)$$

$$\begin{aligned}&-\Phi_2[\rho+\epsilon\delta\rho,z,v,T_c]+\Phi_2[\rho,z,v,T_c]\\ &\qquad = -\int_0^1 \epsilon\delta\rho\left((v+Q)q + \rho(v+Q)q_\rho + q_\rho\int_x^1 \rho q dy\right)dx + o(\epsilon),\end{aligned}$$

$$-\Phi_3[\rho+\epsilon\delta\rho,z,v,T_c]+\Phi_3[\rho,z,v,T_c]$$
$$=-C_f\int_0^1\epsilon\delta\rho\left(\frac{(v+Q)^2}{2}+q_\rho\int_x^1\rho(v+Q)dy\right)dx+o(\epsilon),$$

$$-\Phi_4[\rho+\epsilon\delta\rho,z,v,T_c]+\Phi_4[\rho,z,v,T_c]$$
$$=-C_c\int_0^1\epsilon\delta\rho\left((v+Q)+q_\rho\int_x^1\rho dy\right)dx+o(\epsilon).$$

Then Φ_ρ is

$$\Phi_\rho[\delta\rho;\rho,z,v,T_c]=-\int_0^1\delta\rho\left(\rho(v+Q)q_\rho+q_\rho R(0)S(x)-\frac{\phi}{\rho}\right)dx$$
$$-\int_0^1 R(x)[\delta\rho\ q_\rho]_t dx$$

with

$$\phi[\rho,z,v,T_c]:=-\left(\rho Q_t+\rho(v+Q)q+C_f\rho\frac{(v+Q)^2}{2}+C_c\rho(v+Q)\right).$$

Before finalizing the ξ_v-integral, we have to integrate by parts in order to get rid of the time derivative of the perturbation $\delta\rho$ in the term (4.26).

$$
\begin{aligned}
&- \int_0^{t_{\text{end}}}\int_0^1 \xi_v \frac{R(x)}{R(0)}[\epsilon\delta\rho\ q_\rho]_t dxdt \\
&= \int_0^{t_{\text{end}}}\int_0^1 \epsilon\delta\rho\ q_\rho \left[\xi_v \frac{R(x)}{R(0)}\right]_t dxdt - \left[\xi_v \frac{1}{R(0)}\int_0^1 \epsilon\delta\rho\ q_\rho R(x)dydx\right]_{t=0}^{t=t_{\text{end}}} \\
&= \int_0^{t_{\text{end}}}\int_0^1 \epsilon\delta\rho\ q_\rho \left[(\xi_v)_t \frac{R(x)}{R(0)} + \xi_v \frac{R_t(x)}{R(0)} - \xi_v \frac{R_t(0)R(x)}{R(0)^2}\right] dxdt \\
&\qquad - \left[\xi_v \frac{1}{R(0)}\int_0^1 \epsilon\delta\rho\ q_\rho R(x)dydx\right]_{t=0}^{t=t_{\text{end}}} \\
&= \int_0^{t_{\text{end}}}\int_0^1 \epsilon\delta\rho\ q_\rho \left[\left(\xi_v S(0) + \int_0^1 \xi_\rho\rho_x + \xi_z z_x dx\right)\frac{R(x)}{R(0)} + \xi_v \frac{R_t(x)}{R(0)}\right. \\
&\qquad \left. - \xi_v \frac{R_t(0)R(x)}{R(0)^2}\right] dxdt - \left[\xi_v \frac{1}{R(0)}\int_0^1 \epsilon\delta\rho\ q_\rho R(x)dydx\right]_{t=0}^{t=t_{\text{end}}} \\
&= \int_0^{t_{\text{end}}}\int_0^1 \epsilon\delta\rho q_\rho \left[\frac{R(x)}{R(0)}\int_0^1 \xi_\rho\rho_x + \xi_z z_x dx\right. \\
&\qquad + \xi_v \frac{1}{R(0)}\left(R(x)S(0) + R_t(x) - \frac{R_t(0)R(x)}{R(0)}\right)\Bigg] dx \\
&\qquad - \left[\xi_v \frac{1}{R(0)}\int_0^1 \epsilon\delta\rho\ q_\rho R(x)dx\right]_{t=0}^{t=t_{\text{end}}} + o(\epsilon)
\end{aligned}
$$

Thus, our ξ_v-integral (4.23) equals

$$
\begin{aligned}
I = &\int_0^{t_{\text{end}}}\int_0^1 \epsilon\delta\rho q_\rho \left[\xi_v \frac{1}{R(0)}\left(-\rho(v+Q) - R(0)S(x) + R(x)S(0)\right.\right. \\
&\left. + R_t(x) - \frac{R_t(0)R(x)}{R(0)}\right) + \frac{R(x)}{R(0)}\int_0^1 \xi_\rho\rho_x + \xi_z z_x dx\Bigg] dxdt \\
&- \int_0^{t_{\text{end}}}\int_0^1 \epsilon\delta\rho\ \xi_v \frac{1}{R(0)}\left(\frac{\Phi}{R(0)} - \frac{\phi}{\rho}\right) dxdt \\
&- \left[\xi_v \frac{1}{R(0)}\int_0^1 \epsilon\delta\rho\ q_\rho R(x)dx\right]_{t=0}^{t=t_{\text{end}}} + o(\epsilon).
\end{aligned} \tag{4.27}
$$

The ξ_{T_c}-integral (4.5)**.**

$$
\begin{aligned}
&- \int_0^{t_{\text{end}}} \xi_{T_c} \left[(T_c)_t + h_c \left(T_c - \int_0^1 \frac{p_0}{\rho + \epsilon\delta\rho} dx \right) \right] dt \\
&+ \int_0^{t_{\text{end}}} \xi_{T_c} \left[(T_c)_t + h_c \left(T_c - \int_0^1 \frac{p_0}{\rho} dx \right) \right] dt \\
&= - \int_0^{t_{\text{end}}} \int_0^1 \epsilon\delta\rho \, \frac{h_c}{\rho^2} \, \xi_{T_c} \, dxdt + o(\epsilon)
\end{aligned} \tag{4.28}
$$

The summary of the first variation of $\mathcal{L}$ with respect to ρ. Since everything is prepared, we can start with the derivative. Putting the terms (4.21),(4.22),(4.27) and (4.28) together, we obtain:

$$
\begin{aligned}
\frac{\partial \mathcal{L}(W, z_l, \Lambda)}{\partial \rho}(\delta\rho) = \lim_{\epsilon \to 0} \frac{1}{\epsilon} \Bigg[& \int_0^{t_{\text{end}}} \int_0^1 \epsilon\delta\rho \left((\xi_\rho)_t + (v+Q)(\xi_\rho)_x - q_\rho F \right) dxdt \\
& + \int_0^{t_{\text{end}}} \int_0^1 \epsilon\delta\rho \left(-\xi_v \frac{1}{R(0)} \left(\frac{\Phi}{R(0)} - \frac{\phi}{\rho} \right) - z K'_\rho(\rho) \xi_z - \frac{h_c}{\rho^2} \xi_{T_c} \right) dxdt \\
& - \left[\int_0^{t_{\text{end}}} \epsilon\delta\rho (v+Q) \xi_\rho dt \right]_{x=0}^{x=1} - \left[\xi_v \frac{1}{R(0)} \int_0^1 \epsilon\delta\rho \; q_\rho R(x) dx \right]_{t=0}^{t=t_{\text{end}}} \\
& - \int_0^{t_{\text{end}}} \epsilon\delta\rho(0,t) \eta_\rho dt - \int_0^1 \epsilon\delta\rho(x,0) \eta_\rho dx + o(\epsilon) \Bigg],
\end{aligned}
$$

where F is defined as

$$
\begin{aligned}
F[\rho, z, v, T_c, \xi_\rho, \xi_z, \xi_v] := \xi_\rho \rho + \int_x^1 \xi_\rho \rho_x + \xi_z z_x dy - \frac{R(x)}{R(0)} \int_0^1 \xi_\rho \rho_x + \xi_z z_x dx \\
+ \xi_v \frac{1}{R(0)} \left(\rho(v+Q) + R(0) S(x) - R(x) S(0) - R_t(x) + \frac{R_t(0) R(x)}{R(0)} \right).
\end{aligned}
$$

By using that $\delta\rho$ is arbitrary, we end up with

$$
\boxed{ -(\xi_\rho)_t - (v+Q)(\xi_\rho)_x = -q_\rho F - \xi_v \frac{1}{R(0)} \left(\frac{\Phi}{R(0)} - \frac{\phi}{\rho} \right) - z K'_\rho(\rho) \xi_z - \frac{h_c}{\rho^2} \xi_{T_c} } \tag{4.29}
$$

with the terminal condition

$$
\boxed{ \xi_\rho = 0 \quad \text{for} \;\; t = t_{\text{end}} } \tag{4.30}
$$

and boundary condition

$$
\boxed{ \xi_\rho (v+Q) = 0 \quad \text{for} \;\; x = 1 } \tag{4.31}
$$

REMARK 4.1. *Note that we will have a problem evaluating the boundary condition for x_1, if the velocity $u = v+Q$ at $x = 1$ would vanish at some time. We therefore have to assume positive velocities at $x = 1$ for all times $t \in (0, t_{end}]$. The only exception will be at $t = 0$, where we will have $u(x, 0) = 0$ in the case of an engine start. We will extrapolate the boundary condition for ξ_ρ for this time.*

4.4. Coupling conditions for the adjoint equations. Now, let us discuss the derivation of coupling conditions for the adjoint equations. Let us consider the first variation of the Lagrangian for the whole network (4.1-4.10) with respect to the density in the i-th pipe and considering only the term at the boundaries of the pipe, we obtain:

$$0 \stackrel{!}{=} \frac{\partial \mathcal{L}(W, z_l, \Lambda)}{\partial \rho^i}(\delta\rho) = -\int_0^{t_{\text{end}}} \delta\rho^i(L^i, t)\left((v^i(t) + Q^i(L^i, t))\xi_\rho^i(L^i, t) + \zeta_\rho^{i+1}(t)\right) dt + \int_0^{t_{\text{end}}} \delta\rho^i(0, t)\left((v^i(t) + Q^i(0, t))\xi_\rho^i(0, t) + \zeta_\rho^i(t)\right) dt.$$

Using the fact that $\delta\rho^i$ is arbitrary, we obtain

$$(v^i(t) + Q^i(L^i, t))\xi_\rho^i(L^i, t) = -\zeta_\rho^{i+1}(t) \tag{4.32}$$

and

$$(v^i(t) + Q^i(0, t))\xi_\rho^i(0, t) = -\zeta_\rho^i(t). \tag{4.33}$$

So increasing the indices of all terms in (4.33), we can write together with (4.32):

$$(v^i(t) + Q^i(L^i, t))\xi_\rho^i(L^i, t) = -\zeta_\rho^{i+1}(t) = (v^{i+1}(t) + Q^{i+1}(0, t))\xi_\rho^{i+1}(0, t). \tag{4.34}$$

4.5. Summary - The optimality system. We want to summaries the results of all computation in this section. Our optimality system now consists of

constraints or state equations.

$$\boxed{\begin{aligned} \rho_t^i + (v^i + Q^i)\rho_x^i &= -q^i\rho^i, \\ z_t^i + (v^i + Q^i)z_x^i &= -\chi^i z^i K(T^i), \\ v_t^i &= \Phi^i/R^i(0), \\ (T_c^j)_t &= -h_c(T_c^j - T_{\text{Gas}}^j) \end{aligned}} \tag{4.35}$$

for all pipes $i = 1, \ldots, n_P, j \in I_{cc}$ and $(x, t) \in (0, L^i) \times (0, t_{\text{end}})$, with closing relation

$$\rho^i(x, t)T^i(x, t) = p_0 \tag{4.36}$$

for all pipes $i = 1, \ldots, n_P$ and $(x, t) \in [0, L^i] \times [0, t_{\text{end}}]$, initial conditions

$$\boxed{\rho^i(x, 0) = \rho_{ic}^i(x), \quad z^i(x, 0) = z_{ic}^i(x), \quad v^i(0) = v_{ic}^i \quad T_c^j(0) = T_{c\,ic}^j} \tag{4.37}$$

for all pipes $i = 1, \ldots, n_P, j \in I_{cc}$ and $x \in [0, L^i]$, boundary conditions

$$\boxed{\rho^1(0, t) = \rho_l(t), \quad z^1(0, t) = z_l(t)} \tag{4.38}$$

for all times $t \in [0, t_{\text{end}}]$ and coupling conditions

$$\boxed{\rho^{i-1}(L^{i-1},t) = \rho^i(0,t), \quad z^{i-1}(L^{i-1},t) = z^i(0,t)} \tag{4.39}$$

for all pipes $i = 2, \dots, n_P$ and times $t \in [0, t_{\text{end}}]$, where

$$\begin{aligned}
q^i[\rho^i, z^i, T_c^i](x,t) :=& \frac{1}{\gamma p_0}\big[-h(T^i(x,t) - T^i_{\text{Wall}}(x,t)) \\
&+ \chi^i\left(-h_c(T^i(t) - T_c^i(t)) + q_0\rho^i(x,t)z^i(x,t)K(T^i(x,t))\right)\big], \\
T^i_{\text{Wall}}(x,t) :=& \frac{1}{2}\left(T^i(x,t) + T_{out}\right), \\
T^i_{\text{Gas}}(t) :=& \frac{1}{L^i}\int_0^{L^i} T^i(x,t)dx, \\
K(T^i) :=& \frac{\tilde{K}_0 x_r}{u_r}\exp\left(-\frac{E^+}{T_r T^i}\right) = \frac{\tilde{K}_0 x_r}{u_r}\exp\left(-\frac{E^+}{T_r p_0}\rho^i\right) =: K_\rho(\rho^i), \\
(R^i(x))(t) :=& \int_x^{L^i} \rho^i(y,t)dy,
\end{aligned}$$

$$\begin{aligned}
\Phi^i[\rho^i, z^i, v^i, T_c^i](t) :=\ & p^i_{1l}(t) - p^i_{1r}(t) - \int_0^{L^i} \rho^i(x,t)Q^i_t(x,t)dx \\
&- \int_0^{L^i} \rho^i(x,t)(v^i(t) + Q^i(x,t))q^i(x,t)dx \\
&- C_f\int_0^{L^i} \rho^i(x,t)\frac{(v(t)^i + Q^i(x,t))^2}{2}dx \\
&- \chi^i C_c\int_0^{L^i} \rho^i(x,t)(v^i(t) + Q^i(x,t))\ dx.
\end{aligned}$$

adjoint or co-state equations.

$$\boxed{\begin{aligned}
-(\xi^i_\rho)_t - (v^i + Q^i)(\xi^i_\rho)_x =& -q_{\rho^i}F^i - \chi^i\left(z^i K'_\rho(\rho^i)\xi^i_z + \frac{h_c}{(\rho^i)^2 L^i}\xi^i_{T_c}\right) \\
&- \xi^i_v\frac{1}{R^i(0)}\left(\frac{\Phi^i}{R^i(0)} - \frac{\phi^i}{\rho^i}\right), \\
-(\xi^i_z)_t - (v^i + Q^i)(\xi^i_z)_x =& -q^i_z F^i - \xi^i_z\left(\chi^i K(T^i) - q^i\right) \\
-(\xi^i_v)_t =& -\xi^i_v S^i(0) - \int_0^{L^i} \xi^i_\rho\rho^i_x + \xi^i_z z^i_x dx \\
-(\xi^j_{T_c})_t =& -\int_0^{L^j} q_{T_c^j}F^j dx - h_c\xi^j_{T_c} + (T_c^j - T_{opt})
\end{aligned}} \tag{4.40}$$

for all pipes $i = 1, \dots, n_P, j \in I_{cc}$ and $(x,t) \in (0, L^i) \times (0, t_{\text{end}})$, with terminal conditions

$$\boxed{\xi^i_\rho(x, t_{\text{end}}) = 0, \quad \xi^i_z(x, t_{\text{end}}) = 0, \quad \xi^i_v(t_{\text{end}}) = 0, \quad \xi^j_{T_c}(t_{\text{end}}) = 0} \tag{4.41}$$

for all pipes $i = 1, \dots, n_P, j \in I_{cc}$ and $x \in [0, L^i]$, boundary conditions

$$\boxed{\begin{aligned} &\xi^{n_P}_1(L^{n_P}, t)(v^{n_P}(t) + Q^{n_P}(L^{n_P}, t)) = 0, \\ &\xi^{n_P}_2(L^{n_P}, t)(v^{n_P}(t) + Q^{n_P}(L^{n_P}, t)) = 0 \end{aligned}} \tag{4.42}$$

for all times $t \in [0, t_{\text{end}}]$, and coupling conditions

$$\boxed{\begin{aligned} &(v^i(t) + Q^i(L^i, t))\xi^i_\rho(L^i, t) = (v^{i+1}(t) + Q^{i+1}(0, t))\xi^{i+1}_\rho(0, t), \\ &(v^i(t) + Q^i(L^i, t))\xi^i_z(L^i, t) = (v^{i+1}(t) + Q^{i+1}(0, t))\xi^{i+1}_z(0, t) \end{aligned}} \tag{4.43}$$

for all pipes $i = 1, \dots, n_P$ and times $t \in [0, t_{\text{end}}]$, where

$$\begin{aligned}
q^i_{T_c} &:= \chi^i \frac{h_c}{\gamma p_0},\\
q^i_z[\rho^i](x,t) &:= \chi^i \frac{q_0}{\gamma p_0} \rho^i K(T^i(x,t)),\\
q^i_\rho[\rho^i, z^i, T^i_c](x,t) &:= \frac{1}{\gamma p_0}\Bigg(\frac{h + \chi^i h_c}{(\rho^i(x,t))^2} + \chi^i q_0 z^i(x,t)\rho^i(x,t) K'_\rho(\rho^i(x,t)\\
&\quad + \chi^i K_\rho(\rho^i(x,t)))\Bigg),
\end{aligned}$$

$$\begin{aligned}
\phi^i[\rho^i, z^i, v^i, T^i_c](x,t) &:= -\Bigg(\rho^i(x,t) Q^i_t(x,t) + \rho^i(x,t)(v^i(t) + Q^i(x,t)) q^i(x,t)\\
&\quad + C_f \rho^i(x,t) \frac{(v^i(t) + Q^i(x,t))^2}{2}\\
&\quad + \chi^i C_c \rho^i(x,t)(v^i(t) + Q^i(x,t))\Bigg),\\
(S^i[\rho^i, z^i, v^i, T^i_c](x))(t) &:= \frac{1}{(R^i(0))(t)} \int_x^{L^i} \Bigg(\rho^i(y,t) q^i(y,t)\\
&\quad + C_f \rho^i(y,t)(v^i(t) + Q^i(y,t)) + \chi^i C_c \rho^i(y,t)\Bigg) dy,\\
F^i[\rho^i, z^i, v^i, T^i_c, \xi^i_\rho, \xi^i_z, \xi^i_v](x,t) &:= \xi^i_\rho(x,t)\rho^i(x,t) + \int_x^{L^i} \xi^i_\rho(y,t)\rho^i_x(y,t) + \xi^i_z(y,t) z^i_x(y,t) dy\\
&\quad - \frac{(R^i(x))(t)}{(R^i(0))(t)} \int_0^{L^i} \xi^i_\rho(x,t)\rho^i_x(x,t) + \xi^i_z(x,t) z^i_x(x,t) dx\\
&\quad + \xi^i_v(t) \frac{1}{(R^i(0))(t)} \Bigg(\rho^i(x,t)(v^i(t) + Q^i(x,t))\\
&\qquad + (R^i(0))(t)(S^i(x))(t) - (R^i(x))(t)(S^i(0))(t)\\
&\qquad - (R^i_t(x))(t) + \frac{(R^i_t(0))(t)(R^i(x))(t)}{(R^i(0))(t)}\Bigg).
\end{aligned}$$

Furthermore, since we will be interested in the quantity η_z, the relation

$$\boxed{\xi^1_z(0,t)(v^1(t) + Q^1(0,t)) = \eta_z(t)} \tag{4.44}$$

for all $t \in [0, t_{\text{end}}]$ is needed.

optimality condition.

$$\boxed{(\sigma + \eta_z)(z^*_l - z_l) \geq 0 \quad \forall\ 0 \leq z^*_l \leq z^{\max}_l} \tag{4.45}$$

for all $t \in (0, t_{\text{end}})$.

5. Discretization. We follow the first optimize-then-discretize approach to numerically calculate a solution to the necessary optimality conditions. In particular, the calculated discretized adjoint converges to the continuous adjoint, thus smallness of the calculated gradient is related to smallness of the real gradient. On the other hand, as it is well known, this approach has the draw back, that the calculated discretized gradient of the functional need not coincide with the gradient of the discretized functional. This in turn allows our calculated "descend directions" to fail giving descent for the discretized functional. However, if this happens any further iteration on the given discretization is misleading anyway, since discretization errors become dominant so that a refinement of the discretization is warranted. Hence failure of convergence without nearly satisfied optimality conditions serves us as a cheap estimate for the accuracy of the applied discretization, for more details see Table 5.2 and the discussion in Section 5.3.

For the discretization of the state equation (4.35) an explicit upwind scheme for the spatial differential operator and explicit Euler for the time derivative is used (see [6] for details). Since the adjoint system (4.40) is posed backwards in space and time, we first substitute the time and space variables by $\hat{t} := t_{\text{end}} - t$ and $\hat{x} = L^i - x$. Then the same numerical schemes that we use for solving the state system is used for the solution of (4.40).

By the operation "$\cdot$" between two element of $\mathbb{R}^M$ we mean the weighted scalar product, which is our approximation for the L_2 scalar product, i.e., for two mappings $\varphi, \psi : [0,1] \to \mathbb{R}$ and their discretizations $\varphi_h, \psi_h \in \mathbb{R}^M$ we have

$$\varphi_h \cdot \psi_h = \frac{1}{M} \sum_{m=1}^{M} (\varphi_h)_m (\psi_h)_m \approx (\varphi, \psi)_{L_2} = \int_0^1 \varphi \psi dy, \tag{5.1}$$

noting that we have uniform step sizes.

In order to avoid too many sub-indices, we will not discriminate between the continuous and discrete state, adjoint and control variables, as we will always work with the discrete quantities in this section. Discretization of functionals such as $j : L_1 \to \mathbb{R}$, will be denoted by the sub-index h, i.e., $j \approx j_h$.

5.1. Algorithm. We will have two stopping criteria.

1. `STOP` if the optimality condition $||j'||_{L_2} \approx \frac{1}{M}||\nabla j_h||_2 < TOL_{opt}$ with a tolerance $TOL_{opt} > 0$ and ∇j_h being the discretized projected gradient, i.e.,

$$(\nabla j_h)_m = \begin{cases} \sigma + (\eta_z)_m & 0 \le (z_l)_m \le z_l^{\max}, \\ \min(0, \sigma + (\eta_z)_m) & (z_l)_m = 0, \\ \max(0, \sigma + (\eta_z)_m) & (z_l)_m = z_l^{\max}. \end{cases} \tag{5.2}$$

2. `STOP` if the evaluation of the cost functional do not change any more, i.e., $|j(z_l^k) - j(z_l^{k+1})| < TOL_{diff}$, with a tolerance $TOL_{diff} > 0$.

The first criterion is related to almost satisfied KKT conditions. The second criterion, however, can occur whenever the step size $z_l^{(k)} - z_l^{(k+1)}$ tends to zero. This is the case, in particular, when the computed continuous gradient and the discrete gradient are too far apart. Thus if the algorithm stops due to the second criteria a refinement of the discretization is reasonable to assert convergence of the gradient used to determine the search direction.

Algorithm 5.1.

Guess a initial control $z_l^{(0)} \in \mathbb{R}^M$, where M is the number of grid points in time.

	$\sigma = 0.01$			$\sigma = 10$		
N	DQ_h	$\nabla j_h(z_l) \cdot \delta z_l$	E_ϵ	DQ_h	$\nabla j_h(z_l) \cdot \delta z_l$	E_ϵ
50	-85.3	-2052.5	1967.1	1579.7	-387.4	1967.1
100	-91.8	-1964.9	1873.1	1573.2	-299.9	1873.1
200	-93.9	-1876.2	1782.3	1571.1	-211.2	1782.3
400	-94.9	-1835.9	1741.1	1570.1	-170.9	1741.1
800	-95.4	-1810.9	1715.5	1569.6	-145.9	1715.5
1600	-95.7	-1798.5	1702.7	1569.3	-133.5	1702.7

TABLE 5.1
Difference quotient (DQ_h) vs. discretized analytic gradient ($\nabla j_h(z_l) \cdot \delta z_l$) for $\epsilon = 1$ and $z_l = 0.1$

For $k = 0, 1, 2, \ldots$ repeat the following steps until one of the above stopping criteria is fulfilled:

1. *solve the constraints with control $z_l^{(k)}$ to obtain the corresponding state variables $\rho^{(k)} = \rho(z_l^{(k)}), z^{(k)} = z(z_l^{(k)}), v^{(k)} = v(z_l^{(k)}), T_c^{(k)} = T_c(z_l^{(k)})$;*
2. *solve the adjoint system with state variables $\rho^{(k)}, z^{(k)}, v^{(k)}, T_c^{(k)}$ to obtain the adjoint variables $\xi_\rho^{(k)}, \xi_z^{(k)}, \xi_v^{(k)}, \xi_{T_c}^{(k)}, \eta_z^{(k)}$;*
3. *use $\eta_z^{(k)}$ to compute reduced gradient $\nabla j_h(z_l^{(k)})$, with*

$$\nabla j_h(z_l^{(k)}) = \sigma + \eta_z^{(k)} \in \mathbb{R}^M; \tag{5.3}$$

4. *compute step length α via projected line search (Armijo rule applied to $j_h(z_l)$);*
5. *set $z_l^{(k+1)} = \min(z_l^{\max}, \max(0, z_l^{(k)} - \alpha \nabla j_h(z_l^{(k)})))$ pointwise.*

5.2. Numerical Test: continuous VS discrete gradient. In a first step, we test whether our implementation is correct. In particular, we test the implementation of the derivatives of j_h, as we use them as stopping criteria in our algorithm. To do so we compare directional derivatives with difference approximations, i.e., we check

$$E_\epsilon = |DQ_h - \nabla j_h(z_l) \cdot \delta z_l| = \left| \frac{j_h(z_l + \epsilon \delta z_l) - j_h(z_l)}{\epsilon} - \nabla j_h(z_l) \cdot \delta z_l \right| \to 0$$

for various values of ϵ. In Table 5.1 we calculated these for the values $(\delta z_l)_m = 1$ for all $m = 1, \ldots, M$ (unscaled $(\delta \tilde{z}_l)_m = 0.1$) for various values of spatial grid points N. Due to the CFL-condition, this leads also to a refinement of the time mesh, i.e., $M = \mathcal{O}(N)$, where M is the number of time grid points.

As we can see in Table 5.1 the difference quotient for $\epsilon = 1$ is relatively stable with respect to the mesh size, however the calculated derivatives are still sensitive to mesh refinement. This immediately implies that even at $N = 1600$ we will have to expect effects of unresolved derivatives in our optimization algorithms. On the other hand, by comparing the subtables for $\sigma = 0.01$ and $\sigma = 10$. It is immediately clear from this, that any numerical test for the correct implementation of the derivative will require a much more refined mesh in space and time.

To avoid this problem, we note that the discretization error gets smaller if the end time t_{end} is chosen smaller. In Figure 5.1, we see the behavior of the error between

directional derivatives and difference quotients for various choices of simulation times t_{end}. As it is to be expected, for all values of t_{end} as ϵ decreases so does the error as $E_\epsilon = \mathcal{O}(\epsilon)$. As standard numerical analysis reveals, at some point round-off errors become dominant leading to a behavior $E_\epsilon = \mathcal{O}(\epsilon^{-1})$ as it can be seen in the graphic. We can see clearly that the point where round-off errors become dominate travels to larger ϵ as t_{end} growth. However, at small final times, we can see clearly that the error is small. Since the only change in the program is switching the value for the final time we conclude that our implementation yields correct values for the derivatives.

REMARK 5.2. *The reason why the error E_ϵ in table 5.1 is constant for different values of σ, is that for all $\epsilon > 0$ it holds*

$$\begin{aligned}
\epsilon E_\epsilon &= |j_h(z_l + \epsilon\delta z_l) - j_h(z_l) - \epsilon\nabla j_h(z_l)\cdot\delta z_l| \\
&= \left| j_h^{T_c}(z_l + \epsilon\delta z_l) - j_h^{T_c}(z_l) + \sigma\frac{\epsilon}{M}\sum_{m=1}^{M}(\delta z_l)_m - \frac{\epsilon}{M}\sum_{m=1}^{M}(\sigma + (\eta_z)_m)(\delta z_l)_m \right| \\
&= \left| j_h^{T_c}(z_l + \delta z_l) - j_h^{T_c}(z_l) - \frac{\epsilon}{M}\sum_{m=1}^{M}(\eta_z)_m(\delta z_l)_m \right|,
\end{aligned}$$

and thus, E_ϵ is independent of σ. Above, we denoted

$$j_h^{T_c}(z_l) := \sum_{i\in I_{cc}}\left(\frac{1}{2M}\sum_{m=1}^{M}(T_c^i)_m - T_{opt})^2\right) \approx \sum_{i\in I_{cc}}\frac{1}{2}\int_0^{t_{end}}(T_c^i - T_{opt})^2 dt.$$

5.3. Numerical Test: Convergence Failure and Refinement of Discretization. As a next test, we come back to out statement at the beginning of Section 5. To this end, we consider the behavior of Algorithm 5.1 with the same initial value $z_l^{(0)} = 0$ and $\sigma = 0.01$ for two different spatial (and thus also temporal) refinements.

As we can see from Table 5.2, already in the first iteration slight differences in the value of the cost functional are visible. Already after the third iteration the value of the cost functional is almost unchanged during the application of Algorithm 5.1 for $N = 50$. However, the projected gradient is still large, i.e., $\frac{1}{M}\|\nabla j_h\|_2 \geq 5\cdot 10^{-3}$. On the other hand when $N = 1600$ we can continue until $\frac{1}{M}\|\nabla j_h\|_2 \approx 5\cdot 10^{-4}$ with significantly lower value of j before the cost functional is again stagnant. This confirms our expectation on the convergence of the algorithm and the possible cure of lack of convergence by means of refinement.

6. Numerical Examples. We want to show results of two optimization problems we have simulated.

1. **Setting:** High cost of control, high starting control.
   Expectation: A decrease of ratio of unbrunt gas z_l is more important that achieving an optimal temperature in the catalysts.
2. **Setting:** Low cost of control, low starting control.
   Expectation: The ratio of unbrunt gas z_l should be increased in order to reach optimal temperature in the catalysts.

For all simulation, that we will present in this section, the following holds:

- The geometry of the pipe which is used in these simulations, is presented in the figure 6.1 (for data of the pipe's geometry see Table A.1 in the appendix A).

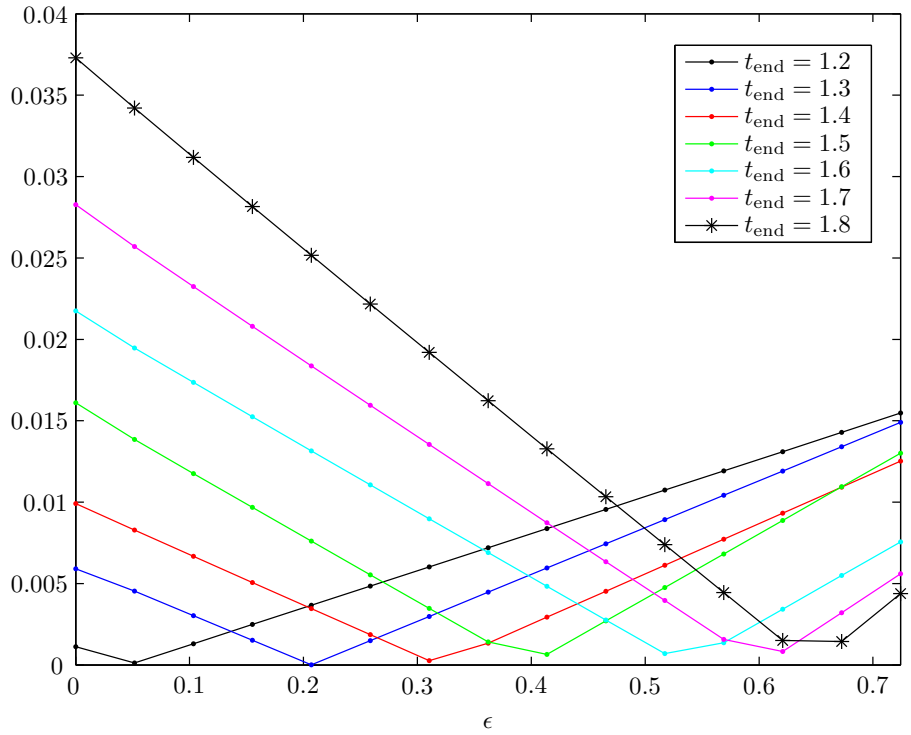

FIGURE 5.1. *Error between gradient and difference quotient*

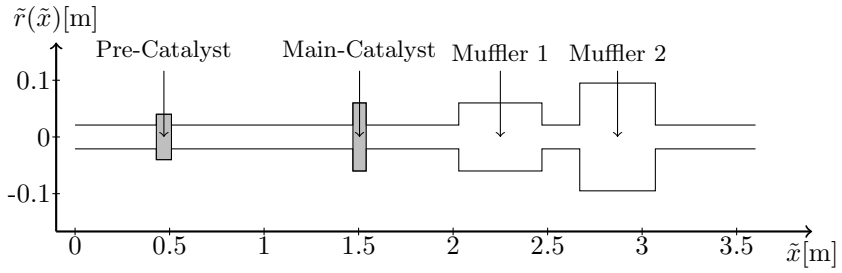

FIGURE 6.1. *Geometry of the exhaust pipe*

- We choose $N = 1600$ to be the number of spatial grid points. The number of gird points in time M depend upon the CFL-condition, and therefore upon the reached velocities in the simulation.
- All quantities presented in this section are unscaled, i.e., they have a dimension. We will denote the unscaled quantities by the tilde symbol " ˜ ". The table of reference values, we used for the scaling can be found in the Table A.2 in the appendix.
- The value of the parameters used for the simulation are listed in the Table A.3 in the appendix.
- For the verification of the simulation results, one should keep in mind the

	$N = 50$		$N = 1600$	
iteration	j_h	$\frac{1}{M}\|\|\nabla j_h\|\|_2$	j_h	$\frac{1}{M}\|\|\nabla j_h\|\|_2$
0	198.2154	0.0613	169.9120	0.0093
1	109.9411	0.0241	98.0908	0.0035
2	39.3864	0.0063	28.5489	0.0005
3	39.2464	0.0060	26.8061	0.0012
4	39.2349	0.0057	26.1496	0.0003
5	39.2349	0.0057	25.8218	0.0014
6	-	-	24.2810	0.0009
7	-	-	23.8705	0.0006
8	-	-	23.8574	0.0004
9	-	-	23.8574	0.0004

TABLE 5.2

Results of the optimization algorithm for different number of spatial grid points N (Values are rounded to five decimal places)

optimal temperature in the catalytic converters

$$\tilde{T}_{opt} = 800\text{K}.$$

- We will observe the temperature in the catalytic converters during the first

$$\tilde{t}_{\text{end}} = 60\text{s}$$

after the engine start.
- The upper bound for the control variable $\tilde{z}_l$ will be

$$\tilde{z}_l^{\max} = 0.5.$$

- The initial condition below correspond to an engine start. For all pipes $i = 1, \dots, 9$ and for all $\tilde{x} \in [0, \tilde{L}^i]$

$$\begin{aligned} &\tilde{\rho}_{ic}^i(\tilde{x}, 0) = 1.2\frac{\text{kg}}{\text{m}^3}, \quad \tilde{z}_{ic}^i(\tilde{x}, 0) = 0, \\ &\tilde{u}_{ic}^i(\tilde{x}, 0) = 0\frac{\text{m}}{\text{s}}, \qquad \tilde{T}_{c\,ic}^i(0) = 290.28\text{K}. \end{aligned} \tag{6.1}$$

Note that these are the physical and not mathematical initial condition for this problem. We need for our mathematical model (4.35) an initial condition for $\tilde{v}^i$. From the above condition we can derive it by integrating equation (2.4).

$$\begin{aligned} v_{ic}^i = &\int_0^{L^i} u_{ic}^i(x)dx - \int_0^{L^i}\int_0^x \frac{1}{\gamma p_0}\Big[- h(T_{ic}^i(y) - T_{\text{Wall}}^i) \\ &+ \chi^i \left(-h_c(T_{ic}^i(y) - T_{c\,ic}^i) + q_0\rho_{ic}^i(y)z_{ic}^i(y)K(T_{ic}^i(y))\right)\Big]dydx, \end{aligned}$$

So applying ideal gas law for obtaining T_{ic}, we can deduce, that with (6.1), we have

$$\tilde{v}_{ic}^{i}(0) = 0. \tag{6.2}$$

- The boundary condition for the density for all pipes $i = 1, \ldots, 9$ and for all $\tilde{t} \in [0, \tilde{t}_{\text{end}}]$

$$\tilde{\rho}_l(t) = 0.4 \frac{\text{kg}}{\text{m}^3}. \tag{6.3}$$

The pressure boundary conditions $\tilde{p}_l$ and $\tilde{p}_r$ are only physical boundary conditions. For the mathematical model (4.35) they are only parameters.
The boundary condition the ratio of unburnt gas (the quantity we want to control optimally) for the two simulations will be announced in the following subsections.

6.1. Example 1: High cost of control, high starting control. The cost of control σ and the value for the first guess of the control variable z_l (the boundary condition for the ratio of unburnt gas) for this simulation were

$$\sigma = 20, \qquad \tilde{z}_l(\tilde{t}) = 0.15 \ \ \forall \tilde{t} \in [0, \tilde{t}_{\text{end}}]. \tag{6.4}$$

The results of the simulation are illustrated in the Table 6.1 and Figure 6.2. The first figure shows the mapping $\tilde{t} \mapsto \tilde{z}_l(\tilde{t})$, where $\tilde{z}_l$ is the boundary condition for the ratio of unburnt gas. The two other mappings show the temperature development over time in the two catalytic converters (pipe 2 and 4). The table shows the evaluation of the cost functional for the iterations done by the algorithm. $\mathcal{J}$ denotes the total cost functional, whereas $\mathcal{J}_z$ and $\mathcal{J}_{T_c^i}$ denote the cost of the control variable z_l and the cost of missing the optimal temperature T_{opt} in the catalysts, respectively. We split the cost functional as follows

$$j_h = \sigma j_h^z + \sum_{l \in I_{cc}} j_h^{T_c^l}, \tag{6.5}$$

$$j_h^z := \frac{t_{\text{end}}}{M} \sum_{m=1}^{M} (z_l)_m \approx \int_0^{t_{\text{end}}} z_l(t) dt, \tag{6.6}$$

$$j_h^{T_c^i} := \frac{t_{\text{end}}}{2M} \sum_{m=1}^{M} ((T_c^i)_m - T_{opt})^2 \approx \frac{1}{2} \int_0^{t_{\text{end}}} (T_c^i(t) - T_{opt})^2 dt. \tag{6.7}$$

The tables contain the scaled quantities, since the unscaled values would be large. The key quantities like relation between initial and final cost and the optimality conditions, will remain their informative value, despite scaling.

We observe that after one iteration the optimization algorithm stops, since the optimality condition is fulfilled. Due the high cost of the control, the optimal solution is $\tilde{z}_l(\tilde{t}) = 0$ for all $\tilde{t} \in [0, \tilde{t}_{\text{end}}]$. This means for our application, that one should use at least the stoichiometric amount of air in the combustion chamber of the engine, i.e., enough air for a complete combustion of the fuel, such that no unburnt gas enters the pipe. In other words, fuel is so expensive, it should not be used for heating up the catalytic converters.

iteration	j_h	j_h^z	$j_h^{T_c^2}$	$j_h^{T_c^4}$	$\frac{1}{M}\|\|\nabla j_h\|\|$
0	**5042.791**	**250**	**17.842**	**24.948**	**0.01698**
1	**169.912**	**0**	**36.764**	**133.149**	**0**

TABLE 6.1

Example 1: Evaluation of the scaled cost functional (rounded to three decimal places) and optimality condition (rounded to five decimal places) for different control variables $\tilde{z}_l$, computed by the optimization algorithm. (Compare figure 6.2 for corresponding control)

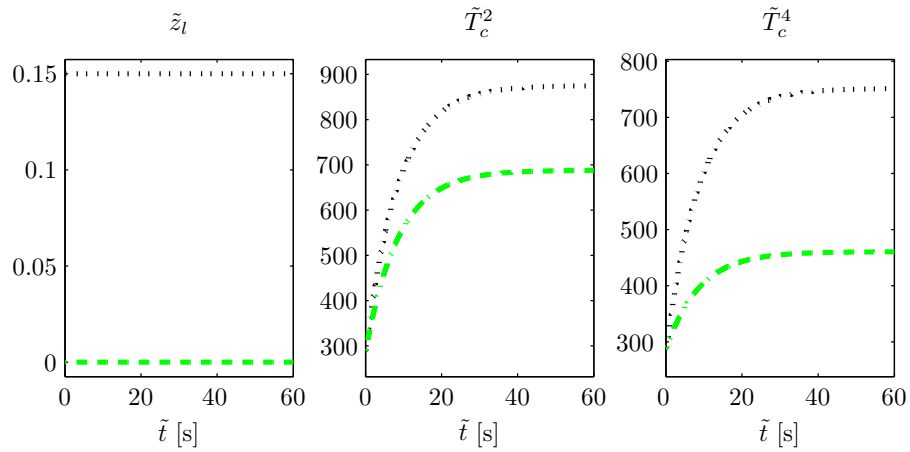

FIGURE 6.2. *Example 1: Boundary condition for ratio of unburnt gas $\tilde{z}$ and temperatures in the catalytic converters $\tilde{T}_c^i$ in [K] for some iterations (Compare table 6.1 for corresponding evaluation of the cost functional)*

In Figure 6.3, we can see the steady state solutions after of the state variables for the initial control (black dotted lines) and the optimal control (green dashed lines). The solid black lines show the geometry of the exhaust pipe and the blue rectangles denote the catalysts.

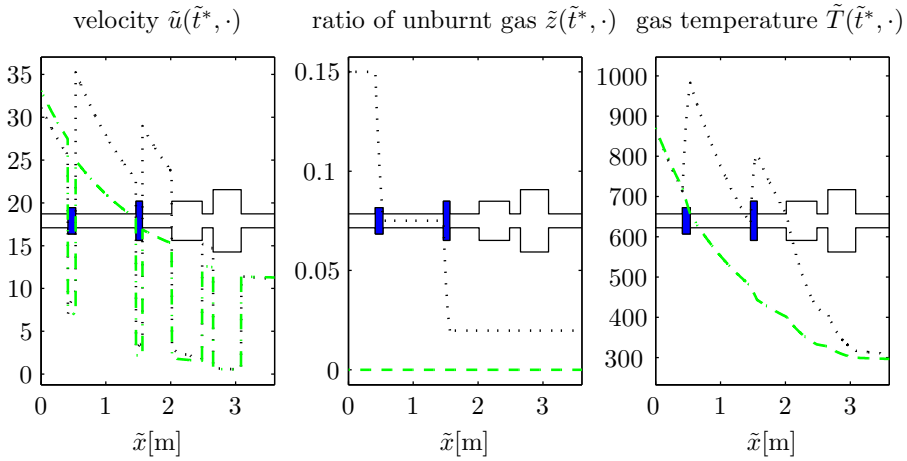

FIGURE 6.3. *Example 1: Results of numerical simulation of the state variables velocity $\tilde{u}$ in $[\frac{m}{s}]$, ratio of unburnt gas $\tilde{z}$ and gas temperature $\tilde{T}$ in $[K]$ at time $\tilde{t}^* = \tilde{t}_{end} = 60s$ (compare colors at table 6.1)*

In the first plot of Figure 6.3, we see the decreasing velocity profile. The reason

for this behavior is the increasing density/decreasing temperature. The changes in diameter of the exhaust pipe lead to changes of the velocity at the junctions. The second plot shows the ratio of unburnt gas in the exhaust pipe. In the first iteration (black dotted line), we have a concentration of 0.15 as the boundary condition for the unscaled ratio of unburnt gas, which decreases in the two catalytic converters during the exothermic reaction. The temperature (third plot) increases in the catalytic converts, in the case in which we have a positive concentration of unburnt gas, and decreases over the whole exhaust pipe due to the heat transfer with the (colder) wall.

6.2. Example 2: Low cost of control, low starting control. The cost of control σ and the value for the first guess of the control variable z_l (the boundary condition for the ratio of unburnt gas) for this simulation are

$$\sigma = 0.01, \qquad \tilde{z}_l(\tilde{t}) = 0 \quad \forall \tilde{t} \in [0, \tilde{t}_{\text{end}}]. \tag{6.8}$$

The results of the simulation are illustrated in the Table 6.2 and Figure 6.4. In this scenario (fuel is cheap), the optimization algorithm suggests to use more of fuel. After 9 iterations this yields to our "optimal" control, although the stopping criteria which led to the abortion of the algorithm, was the second criterion (no change of the cost functional due to 20 line search attempts). Nevertheless, the obtained control leads to a fast heating a temperature close to the optimal $\tilde{T}_{opt} = 800K$ in both catalytic converters, i.e., from the application's point of view: a satisfying result.

iteration	j_h	j_h^z	$j_h^{T_c^2}$	$j_h^{T_c^4}$	$\frac{1}{M}\|\|\nabla j_h\|\|$
0	**169.912**	**0**	**36.765**	**133.148**	**0.00933**
1	**98.091**	**482.276**	**51.327**	**41.941**	**0.00347**
2	**28.549**	**317.238**	**15.390**	**9.986**	**0.00058**
3	26.806	282.716	10.502	13.477	0.00130
4	**26.150**	**333.782**	**14.747**	**8.065**	**0.00035**
5	**25.822**	**266.863**	**8.843**	**14.310**	**0.00139**
6	**24.281**	**283.835**	**9.858**	**11.584**	**0.00091**
7	**23.870**	**295.016**	**10.702**	**10.219**	**0.00061**
8	23.857	302.555	11.346	9.486	0.00042
9	**23.857**	**302.555**	**11.346**	**9.486**	**0.00042**

TABLE 6.2

Example 2: Evaluation of the scaled cost functional (rounded to three decimal places) and optimality condition (rounded to five decimal places) for different control variables z_l, computed by the optimization algorithm. (Compare figure 6.4 for corresponding control; only iteration marked bold are illustrated in the figure.)

7. Conclusion. In this paper, we were able to answer the question, how to ensure reaching an optimal temperature in a catalytic converter of an exhaust pipe after the engine start by controlling ratio of unburnt gas in the gas mixture. This was achieved using the formal continuous adjoint for the calculation of derivatives in a projected gradient algorithm. Numerical examples demonstrate the feasibility of the approach, and show that stagnation of the projected gradient algorithm is due to insufficient resolution of the differential equations and can thus be healed by refinement of the discretization.

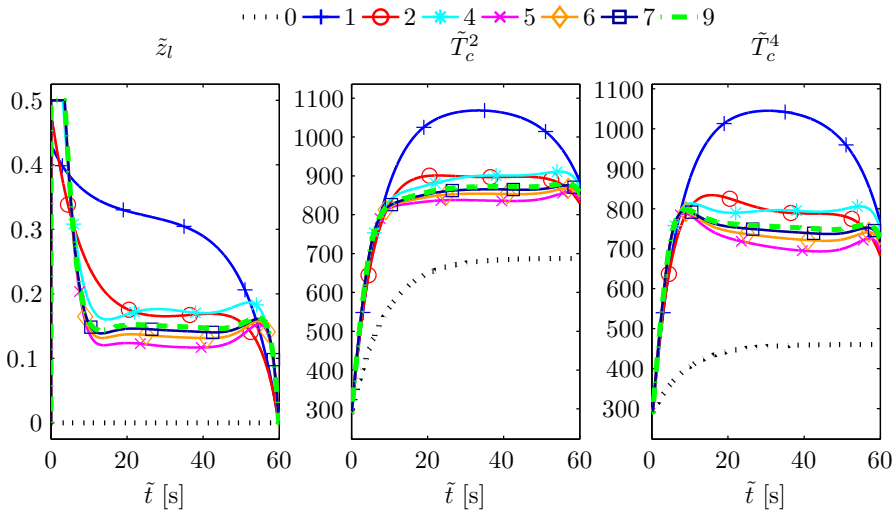

FIGURE 6.4. *Example 2: Boundary condition for ratio of unburnt gas $\tilde{z}$ and temperatures in the catalytic converters $\tilde{T}_c^i$ in [K] for some iterations (Compare table 6.2 for corresponding evaluation of the cost functional)*

REFERENCES

[1] C. CASTRO, F. PALACIOS, AND E. ZUAZUA, *Optimal control and vanishing viscosity for the Burgers equation*, in Integral methods in science and engineering. Vol. 2, Birkhäuser Boston Inc., Boston, MA, 2010, pp. 65–90.

[2] S.S. COLLIS, K. GHAYOUR, M. HEINKENSCHLOSS, M. ULBRICH, AND S. ULBRICH, *Optimal control of unsteady compressible viscous flows*, Internat. J. Numer. Methods Fluids, 40 (2002), pp. 1401–1429.

[3] THE CRANE COMPANY, *Flow of Fluids Through Valves, Fittings, and Pipe - Technical Paper No. 410*, Crane Valves, 1982.

[4] G. D'ERRICO, G. FERRARI, AND A. ONORATI, *Numerical modeling of unsteady reacting flows in the exhaust system of a s.i. engine including the catalytic converter*, in Seoul 2000 FISITA World Automotive Congress, 2000.

[5] M. FRANK, A. KLAR, AND R. PINNAU, *Optimal control of glass cooling using simplified pn theory*, Transport Theory and Statistical Physics, 39 (2010), pp. 282–311.

[6] I. GASSER AND M. RYBICKI, *Modelling and simulation of gas dynamics in an exhaust pipe*, Applied Mathematical Modelling, 37 (2013), pp. 2747–2764.

[7] I. GASSER, M. RYBICKI, AND W. WOLLNER, *Modelling, simulation and optimization of gas dynamics in an exhaust pipe*, Proceedings of HYP 2012, (submitted 2012).

[8] M. GUGAT, M. HERTY, A. KLAR, AND G. LEUGERING, *Optimal control for traffic flow networks*, Journal of Optimization Theory and Applications, 126 (2005), pp. 589–616.

[9] M. GUGAT, M. HERTY, A. KLAR, G. LEUGERING, AND V. SCHLEPER, *Well-posedness of networked hyperbolic systems of balance laws*, in Constrained Optimization and Optimal Control for Partial Differential Equations, vol. 160, Springer Basel, 2012, pp. 123–146.

[10] M. HERTY AND V. SACHERS, *Adjoint calculus for optimization of gas networks*, Networks and Heterogeneous Media, 2 (2007), pp. 733–750.

[11] M. HORNIKX, W. DE ROECK, AND W. DESMET, *Flow and geometrical effects on radiated noise from exhausts computed by a hybrid extended fourier pstd method*, in 17th AIAA/CEAS Aeroacoustics Conference (32nd AIAA Aeroacoustics Conference), 2011.

[12] V.F. JAKUBAUSKAS AND D.S. WEAVER, *Transverse vibrations of bellows expansion joints – Part I and II*, Journal of fluid and structures, 12 (1998), pp. 445–473.

[13] C. KIRCHNER, M. HERTY, S. GÖTTLICH, AND A. KLAR, *Optimal control for continuous supply network models*, Netw. Heterog. Media, 1 (2006), pp. 675–688.

[14] S.-M. LIANG, S.-J. TSAI, AND S.-F. WANG, *An effective approach for calculation of exhaust pipe flows*, Journal of Mechanics, 25 (2009), pp. 177–188.

[15] S.-M. LIANGA AND S.-M. TAIB, *Analysis and prediction of shock-induced near-field acoustics*

from an exhaust pipe, Computers & Fluids, 45 (2011), pp. 222–232.
[16] S.-F. Ling, T.-C. Pan, G.-H. Lim, and C.-H. Tseng, *Vibration isolation of exhaust pipe under vehicle chassis*, International Journal of Vehicle Design, 15 (1994).
[17] R. Mulley, *Flow of Industrial Fluids - Theory and Equations*, CRC Press, 2004.
[18] R. Natalini and L. Lacoste, *Mathematical modeling of chemical processes in exhaust pipe*, tech. report, IAC Rome, 2004.
[19] R. Petrucci, *Un modello matematico di combustione dei gas di scarico in marmitte catalitiche*, master's thesis, Roma Tre - Universit delgi studi, 2007.
[20] S. Rjasanow, *Heat transfer in an insulated exhaust pipe*, Journal of Engineering Mathematics, 29 (1995), pp. 33–49.
[21] F. Tröltzsch, *Optimal Control of Partial Differential Equations: Theory, Methods, and Applications*, Graduate Studies in Mathematics, American Mathematical Society, 2010.
[22] S. Ulbrich, *A sensitivity and adjoint calculus for discontinuous solutions of hyperbolic conservation laws with source terms*, SIAM J. Control Optim., 41 (2002), pp. 740–797 (electronic).

Appendix A. Data.

$$h := \frac{4\tilde{h}x_r}{\tilde{d}\rho_r u_r c_v}, \quad h_c := \frac{\tilde{h}_c x_r}{\rho_r u_r c_v}, \quad q_0 := \frac{\rho_r z_r \tilde{q}_0 R}{p_r c_v}, \quad C_f := \frac{\tilde{C}_f x_r}{\tilde{d}}, \quad C_c := \frac{\tilde{C}_c x_r}{u_r}. \tag{A.1}$$

The physical boundary conditions for the pressure used in all simulations are

$$\tilde{p}_l = 1.01\text{bar}, \qquad \tilde{p}_r = 1\text{bar}. \tag{A.2}$$

The following tables A.1, A.2 and A.3 contain the information of the pipe's geometry, reference values and parameters used for the simulations, respectively.

pipe number	length [m]	radius [m]	CC
1	0.415	0.021	0
2	0.12	0.04	1
3	0.93	0.021	0
4	0.1	0.06	1
5	0.45	0.021	0
6	0.47	0.06	0
7	0.17	0.021	0
8	0.43	0.095	0
9	0.515	0.021	0
sum	3.6	-	2

Table A.1
Pipe geometry

Quantity	Meaning	Unit	Reference quantity	Reference value
$\tilde{t}$	time	s	$t_r = x_r/u_r$	0.36s
$\tilde{x}$	space	m	$x_r = \tilde{L}$	3.6m
$\tilde{\rho}$	density	kg m^{-3}	ρ_r	1.2 kg m^{-3}
$\tilde{u}$	velocity	m s^{-1}	u_r	10 m s^{-1}
$\tilde{p}$	pressure	kg m^{-1} s^{-2}	p_r	10^5 kg m^{-1} s^{-2}
$\tilde{T}$	temperature	K	$T_r = p_r/(R\rho_r)$	290.28 K
$\tilde{z}$	ratio of unburnt gas		z_r	0.1

TABLE A.2

Reference values

Parameter	Meaning	Unit	Parameter value
$\tilde{C_f}$	wall friction		0.0241
c_v	specific heat at constant volume	m^2 s^{-2} K^{-1}	717.7
$\tilde{h}$	heat transfer rate with wall	kg s^{-3} K^{-1}	100
p_0	scaled pressure in leading order		1
R	ideal gas constant	m^2 s^{-2} K^{-1}	287.08
$\tilde{T}_{out}$	external temperature	K	290.28
γ	adiabatic exponent		1.4
$\tilde{C_c}$	catalyst friction	s^{-1}	800
$\tilde{T}^+$	activation temperature	K	600
$\tilde{h}_c$	heat transfer rate with catalyst	kg s^{-3} K^{-1}	100
$\tilde{K}_0$	reaction rate	s^{-1}	100
$\tilde{q}_0$	heat release rate in catalyst	m^2 s^{-2}	$5 \cdot 10^6$
$\tilde{T}_{opt}$	optimal temperature in catalyst	K	800

TABLE A.3

Parameters, units, parameter values